# ASSESSING THE RELIABILITY OF ELASTIC GEOBAROMETRY METHODS

Bonazzi[1,*], Tumiati[2], Thomas[3], Angel[1], Alvaro[1]

[1]Department of Earth and Environmental Sciences, University of Pavia, Italy

[2] Department of Earth and, University of Milan, Italy

[3]Department of Earth Sciences, Syracuse University, Syracuse, NY 13244, USA

*For submission to:* **Lithos**

*Corresponding author: matteo.alvaro@unipv.it*

## Abstract

Elastic geobarometry makes use of the contrast in elastic proprieties between host inclusion pairs to determine entrapment conditions for the inclusions. The theoretical basis has been developed extensively in the past few years, but an experimental validation and assessment of the calculated P and T of entrapment is still required. We report Raman measurements of quartz inclusions trapped in almandine garnet at eclogitic conditions in a piston cylinder apparatus, from which we determined the stress state in the inclusions by two methods. The use of a hydrostatic calibration of the 464cm$^{-1}$ line of quartz leads to a large spread in inclusion 'pressure' values for inclusions trapped at 3 GPa, although it is more accurate for inclusions trapped at 2.5 GPa. Entrapment pressures calculated via this method can be up to 0.8 GPa in error. The use of the mode Grüneisen tensors of quartz enables the full strain state and thus the stress state of the inclusion to be determined, and leads to a much smaller spread in mean stress values inferred for inclusions, and the calculated entrapment pressures differ from the known experimental values by less than 0.2 GPa. These results show that the most significant effect of the elastic anisotropy of quartz is on the Raman shifts of the inclusion, and not on the subsequent calculation of entrapment conditions.

## 1. INTRODUCTION

Elastic geobarometry makes use of the contrast in elastic proprieties between host inclusion pairs to determine entrapment pressures for the inclusions. When a host-inclusion pair is exhumed from depth to the Earth's surface non-lithostatic stresses are developed in the inclusion because of the contrast in their elastic properties Angel et al. (2015). Current models for elastic geobarometry only can only be applied to the simple case of elastically isotropic host-inclusion pairs with ideal geometries consisting of a small inclusion trapped in an effectively infinite host Angel et al. (2015). Recent work on elastic geobarometric methods allow us to calculate strains from the Raman shifts of multiple Raman-active bands (Murri et al. 2018). Furthermore, the correct analysis for the shape of the inclusion and the geometry of the inclusion has been developed and discussed by Mazzucchelli et al. (2018) and Campomenosi et al. (2018). The elastic anisotropy of the inclusion can also be included following the approach proposed by Mazzucchelli et al. (2019). Despite the intensive development an experimental validation to crosscheck the calculated P and T of entrapment is still required. Such validation cannot come from measurements on inclusions in natural rocks as we do not know the exact P and T of entrapment, especially when there is evidence of over-stepping of equilibrium reaction boundaries (e.g. Spear et al., 2014). An excellent means for this assessment can be obtained from synthetic host-inclusion pairs that can be produced with laboratory apparatus at controlled high-P and T conditions (e.g. Thomas and Spear, 2018).

The important criteria for such experimental verification is the choice of host-inclusion pairs that are relevant for geological applications (e.g. index mineral phases in UHPM rocks) that can also be synthesized in the laboratory. We chose to work on quartz inclusions in garnet because they are very common minerals in eclogitic rocks and their elastic proprieties are relatively well-known. On the samples recovered from high P-T experiments, the inclusion pressures can be determined using Raman spectroscopy combined with knowledge of the elastic behavior of the inclusion mineral. However, there are still several open questions

concerning the exact method to determine "pressures" using Raman spectroscopy for inclusions, such as quartz, that are not elastically isotropic.

In particular, for quartz inclusions the residual or remnant pressure ($P_{inc}$) can be determined in two different ways. One method (e.g. Enami et al., 2007; Ashley et al., 2016; Thomas and Spear, 2018) is to interpret the shifts of the 464 $cm^{-1}$ Raman mode of inclusions toward higher wavenumbers as a "pressure" using the calibration of Schmidt and Ziemann (2000). However, their calibration is obtained from hydrostatic experiments, assuming that the Raman shifts are caused solely by compression of a crystal immersed in a hydrostatic fluid. However, this is not correct for anisotropic inclusions such as quartz, trapped in other minerals. If quartz is trapped in a cubic host such as garnet the inclusion will be subject to isotropic strains imposed by the host and therefore, because it is elastically anisotropic, it will develop deviatoric stresses. The change in the Raman band positions of a mineral is determined by the strain imposed on it (Grüneisen, 1926; Barron et al., 1980; Cantrell, 1980; Angel et al., 2019), and therefore an inclusion crystal will exhibit different Raman shifts from a free crystal subject to hydrostatic pressure. The strains on a quartz inclusion crystal can be determined from the observed Raman shifts by using the mode Grüneisen tensors for quartz (Murri et al., 2018; Angel et al., 2019; Murri et al., 2019). In this study we synthesised quartz inclusions in almandine garnet at known pressures and temperatures and measured their Raman spectra. We calculated the inclusion pressures both via the strains (*c.f.* Murri et al., 2018), and by using the hydrostatic calibration of Schmidt and Ziemann (2000). From these residual inclusion pressures we calculated the entrapment pressures using Eosfit-Pinc (Angel et al., 2017) and compared them to the known synthesis conditions, in order to show the effect of the elastic anisotropy of quartz on the calculation of residual or remnant pressures and consequently of entrapment pressures.

## 2. METHODS

### 2.1. Piston-cylinder experiments

Quartz inclusions in almandine garnet are the results of hydrothermal synthesis in the piston cylinder apparatus at Syracuse University Laboratory. The experiments were performed at 3GPa and 775°C and 2.5GPa and 800 °C, typical eclogitic conditions, with run times between 72 and 96 hours. As starting materials we used an oxide mix of following composition: $SiO_2$ (amorphous), Al $(OH)_3$, FeO, $Fe_3O_4$, $Fe_2O_3$, $FeTiO_3$, and MnO (Alfa Aesar). Details of the oxide mixture are given in the supplementary material (Table s1). In order to ensure excess silica was present, the oxide mixture corresponded to the composition of almandine plus 24% excess silica. An equal volume of distilled water was added to wet the oxide mixture completely following the protocol of Thomas and Spear (2018), and approximately 10-15 mg of mixed oxides were loaded into silver capsules for each experiment. We used the capsule design of Trail et al. (2012) in which the silver capsule of 12.7mm of diameter is formed by two identical parts separated by a platinum disk (150μm thick) placed between the open ends of the half capsules. One half-capsule contained the oxide mixture, and the second contained an FMQ buffer assemblage (see Fig 1 in Thomas and Spear, 2018). We left headspace in both parts of the capsule to avoid contaminating the tops of capsules with their contents. The cell assembly used in these experiments is the salt-pyrex-graphite with MgO filler design of Holland (1980). Temperature was measured with D-type thermocouples ($W_{97}Re_3$–$W_{75}Re_{25}$), situated close to the top of the capsule and was considered accurate to within ~ 10 °C. The pressures in the piston–cylinder hydraulic rams were measured with Enerpac 140 MPa Bourdon-tube gauges with 18-cm-diameter dials. Experiments were cold pressurized to the desired run pressure followed by ramping the temperature at 100°C/minute. Runs were quenched to below 100 °C in less than 60 s by turning off the furnace power. Pressure calibration of the piston cylinder is based on the quartz–coesite phase boundary (Boyd and England, 1960; Kitahara and Kennedy, 1964), using the same assemblies as our experiments. Here we describe the results from two experiments, Alm-1 (T=775°C, P=3GPa) and Alm-2 (T=800°C P=2.5GPa).

### 2.2 Sample quality assessment

After quenching the runs the capsule were opened and successful runs were found to contain a mixture of free single crystals of garnet, and also other minerals, immersed in water. Single crystals were removed

from the capsules and the garnet crystals were mounted in epoxy and polished by removing less than 10µm of garnet material. After polishing the garnet crystals from 60 to 100 µm in diameter (Fig. 1a and 1e). We selected quartz inclusions by optical microscopy and selected only ideal inclusions to measure with Raman spectroscopy. An ideal inclusion has to be isolated in a fracture-free garnet host, whose radius must be at least three times larger than that of the inclusion (Zhang, 1998; Mazzucchelli et al., 2018). Samples were also inspected using back scattered electron (BSE) and characterized by electron microprobe analyses and maps using a JEOL JXA 8200 Superprobe equipped with five wavelength–dispersive (WDS) spectrometers, an energy dispersive (EDS) spectrometer (accelerating potential 15 kV, beam current 15nA), at the Department of Earth Sciences, University of Milan. The phase assemblages of Alm-1 and Alm-2 are identical and show many similarities to some natural HP mineral assemblages, and consist of garnet, quartz, kyanite and ilmenite. The composition of the garnet crystals is almost pure almandine (>99%). Inclusions in garnet were quartz, rutile, kyanite and rarely orthopyroxene or ilmenite. Kyanite inclusions were mostly found as small inclusions in the cores of the garnets. The quartz inclusions range from sub-micrometer spherical inclusions to well-faceted inclusions 15µm in maximum dimension. We observed that the garnet crystals in Alm-1 are slightly larger than those in Alm-2 (see Fig. 1). Quartz included in the garnet hosts of Alm-2 are commonly smaller and more numerous than quartz included in the garnet host of Alm-1.

### 2.3 **Raman spectroscopy measurements**

The inclusions were measured using parallel-polarized Raman spectra in backscattering geometry with a Horiba Jobin-Yvon T64000 triple-monochromator spectrometer (spectral resolution of ~2 $cm^{-1}$, instrumental accuracy in peak positions of ~0.35$cm^{-1}$ and 1µm spot size) with a 532nm green laser. All of the measurements have been carried out at 20°C and room pressure. As standard we used a band of a silicon metal standard whose theoretical peak position is 520.7 $cm^{-1}$. We collected Raman spectra over several days, and several times each day we measured the Raman spectrum of a free quartz crystal to have a reference spectrum in order to have good control over instrumental uncertainties and stability.

Raman spectra were acquired with a laser spot of 1um from the center of inclusions because this is the point where the stress and strain is least disturbed by the shape of the inclusion (Campomenosi et al., 2018).

We measured several inclusions in a single garnet host and on some inclusions we repeated the measurement over several days to estimate the reproducibility of the measurements. Overall, we collected data on more than 20 inclusions per experiment. All inclusion spectra were acquired for 5 acquisitions of 40 seconds each. Raman spectra were fitted using a B-spline as a baseline correction and pseudo-Voigt peak functions with the OriginPro 2018b software. The estimated uncertainties on fitted peak positions were commonly < 0.3 cm. On the quartz included in the almandine we measured the wavenumber shifts of quartz inclusions relative to the line positions of a free quartz crystal at room temperature (see tables 1a and 1b). We generally used the shift of three bands of quartz at 128, 206, 464 $cm^{-1}$ because these bands can be easily resolved from those of almandine.

## 3. RESULTS AND DISCUSSION

### 3.1 Raman wavenumber shift, inclusion pressure and strain

The residual or remnant pressure can be calculated from the Raman spectra collected on quartz inclusions while still trapped in garnet following different procedures. The most widely used in literature is simply based on the shift of one single Raman band as a function of external pressure (e.g. Enami et al., 2007; Ashley et al., 2016; Thomas and Spear, 2018). For the sole purposes of comparison, we calculated the inclusion pressure ($P_{inc}^{464}$) on the selected inclusion adopting the hydrostatic calibration by Schmidt and Ziemann (2000) for the Raman shift of the 464 $cm^{-1}$ band using the flowing equation:

$$P_{inc}^{464}\ (\text{MPa}) = 0.36079 \cdot [(\Delta\omega_P)_{464}]^2 + 110.86 \cdot (\Delta\omega_P)_{464} \quad (1)$$

After fitting of the micro-Raman spectra, the wavenumber shifts have been calculated with respect to the wavenumbers obtained from repeated measurements of the reference quartz crystal in air used as standard. In Fig. 2 the $P_{inc}^{464}$ calculated from all of our measurements on the samples retrieved from both experimental synthesis conditions (see Tables 3a and 3b) are compared with the $P_{inc}$ calculated from the known

entrapment conditions from the isotropic host-inclusion model for spherical inclusions (Angel et al., 2014; Angel et al., 2017). This model ignores the effects of the elastic anisotropy on the variation of the inclusion volume with $P$ and $T$, and the effects of anisotropy on the mutual elastic relaxation of the host and the inclusion. The discrepancy between the $P_{inc}^{464}$ measured and the expected $P_{inc}$ calculated for our synthesis conditions are smaller than 0.2 GPa for the experiment at 2.5GPa and 800°C whereas for the experiment at 3GPa and 775°C the maximum discrepancy is about 0.7 GPa (see Fig. 2b). These discrepancies arise mostly from the incorrect assumption of perfectly hydrostatic conditions for an anisotropic inclusion trapped in a cubic host. Therefore, it is intuitive to understand that the deviations increase with increasing the encapsulation pressures.

We used the same Raman measurements to calculate the strain state ($\varepsilon_1$ and $\varepsilon_3$) of the inclusion via the mode Grüneisen tensors of quartz (Murri et al., 2019) using the Strainman software (Angel et al., 2019). As shown in Fig. 3 in Murri et al. (2018) the slopes of the iso-shift lines for the Raman bands that can be measured on quartz inclusions trapped in almandine garnet are almost parallel to one another and are nearly parallel to the isochors. As consequence the correlation between the values of $\varepsilon_1$ and $\varepsilon_3$ obtained in this way is very high (90-99%). The correlation makes it extremely difficult to determine a unique combination of strains from the measured stresses, and the small differences in Raman peak positions measured from a series of inclusions trapped under the same conditions leads to a spread in strains that lies sub-parallel to the isochors (Fig. 3). To minimize the effects of this correlation we performed a series of tests to select the most reliable bands (at least 3 bands) to be used in the calculations of the strain components. As no significant improvement has been observed using different combination of bands (128, 206, 264, 464, 696, 1162 $cm^{-1}$) with the correlations always greater than 90%, we restricted our analyses to the three bands with consistently small instrumental and fitting uncertainties, i.e. those at 128, 206 and 464 $cm^{-1}$.

From the determined strain components, we calculated normal stress components ($\sigma_1=\sigma_2$ and $\sigma_3$) using the elastic tensor of Wang et al. (2015). From the calculated stresses on the inclusion we calculate the $P_{inc}^{strains}$ as the mean stress, $(2\sigma_1+\sigma_3)/3$. As shown by Wang et al. (2015) the elastic moduli of quartz increase non-

linearly with pressure. For small strains the change in elastic moduli is very small compared to the magnitude of the elastic tensor components at room pressure. Calculations performed with the experimental elasticity tensor at 1.5 GPa overestimates the $P_{inc}$ by about 20-24% with respect the calculation using the tensor at room pressure. We therefore carried out the analyses using the elastic tensor at room pressure. With this calculation the discrepancy between the measured $P_{inc}^{strains}$ and the theoretical $P_{inc}$ calculated with the isotropic model from our synthesis conditions are smaller than 0.1 GPa (Table 3 and Fig. 2). As shown in Fig. 2b no significant improvement has been observed in the distribution of the residual pressures for the inclusions from the low-pressure experiment (Alm-2). They are similar to the deviations obtained from the calculations based on only the shift of the 464cm$^{-1}$ line. Conversely for the high-P experiment (Alm-1), while the deviation from the expected residual pressures using the strain method remains identical to that of the low-P runs, the deviations for the values calculated using the 464 line are more than 7 times larger (e.g. up to 0.7 GPa). These results clearly show that the incorrect estimates of $P_{inc}$ obtained by using the hydrostatic calibration of the 464 cm$^{-1}$ line become worse at higher inclusion pressures.

### 3.2 Calculation of entrapment conditions

From the residual or remnant pressures obtained by the two approaches we calculated inclusion entrapment pressures using non-linear equations of state (EoS) of the host and the inclusion minerals using the EosFit-$P_{inc}$ software (Angel et al., 2017). The following results are based on the isotropic model for both the relaxation and the thermodynamic calculation (see Angel et al., 2014; Angel et al., 2017 for details). As could be expected from the results shown in Fig. 2, the $P_{trap}^{strains}$ (Fig. 4) are in good agreement with the experimental pressures of synthesis for both experiments. In we show the results together with a confidence interval of ± 0.2GPa (shaded area in Fig. 4) that provides an indication of the magnitude of uncertainties on these results calculated from the uncertainties in volume strain ($Vs = 2\varepsilon_1 + \varepsilon_3$) at entrapment conditions. On the other hand, the values of $P_{trap}^{464}$, which are derived from the hydrostatic calibration of the Raman shifts, only agree with the experimental synthesis conditions for the experiment at 2.5 GPa (Fig. 4b). For

the experiment at 3 GPa, although some of the $P_{trap}^{464}$ values are correct, the maximum discrepancy is about 1.2 GPa (Fig. 4a). This spread in pressure is far greater than the expected uncertainties. The difference between $P_{trap}$ calculated using the two approaches is greater for the inclusions whose strains deviate most from those expected for hydrostatic stress (yellow area in Fig. 3), indicating that the source of the errors in $P_{trap}^{464}$ comes from ignoring the non-hydrostatic stresses in the inclusions.

## 4. CONCLUSIONS

Prior to this study, it was not clear how the elastic anisotropy of quartz might affect the estimates of Ptrap of inclusions based on a hydrostatic and isotropic model. There are two contributions from elastic anisotropy to this question. The first is that the Raman shifts of a crystal are determined by the strains and not the pressure or mean stress (e.g. Barron et al., 1982; Angel et al., 2019). Therefore, the Raman shifts from solid anisotropic inclusions such as quartz inside a cubic host mineral such as garnet are not the same as those for a quartz crystal under hydrostatic conditions. Second, the anisotropic stresses and the anisotropic elastic properties will modify both the calculation of the elastic relaxation of the host-inclusion system, and the calculation of the $P_{\text{trap}}$ from the $P_{\text{inc}}$ (Alvaro et al., 2019; Mazzucchelli et al., 2019). Our experimental results, summarised in Fig. 2 and 3, clearly show that the $P_{\text{inc}}$ values inferred from the hydrostatic calibration of the shift of the 464 Raman line are in substantial error when the inclusions are subject to strains that are significantly different from those of a crystal under hydrostatic stress (Fig. 3). Therefore, the determination of $P_{\text{inc}}$ as a mean stress derived from the strains based on the measurement of several Raman lines is much more reliable. Second, the fact that our calculated $P_{trap}^{strains}$ values based on these measured $P_{inc}^{strains}$ are in good agreement with the experimental pressure of synthesis indicates that the effects of the elastic anisotropy of quartz on the calculation from $P_{\text{inc}}$ to $P_{\text{trap}}$ is smaller than the other experimental uncertainties.

Therefore, in order to obtain reliable estimates of $P_{\text{trap}}$ of quartz inclusions, a number of steps are required. First, it is important to select approximately spherical inclusions for which the shape effects are small and

can be corrected (Mazzucchelli et al., 2018). Second, the inclusions must be isolated. Table 3 shows that partially-exposed inclusions (e.g. Grt2_I2) have partially-released stresses (Campomenosi et al., 2018; Mazzucchelli et al., 2018) and the resulting $P_{trap}$ values can be up to 0.8 GPa too small for inclusions entrapped in our experiments at 3 GPa. On the other hand, inclusions that are close to other inclusions (e.g. Grt6_I1 in Table 3a) can exhibit inclusion stresses that are higher than isolated inclusions, and thus give $P_{trap}$ values that are significantly too high. Once suitable inclusions have been identified the Raman shifts of several Raman lines from the inclusion must be measured as precisely as possible. This requires that a reference Raman spectrum is measured at the same time with the same instrument settings from a free quartz crystal in air. The strains in the inclusion should be determined from the changes in Raman shifts by using the mode Grüneisen tensors of quartz (Murri et al., 2018; Angel et al., 2019). The $P_{inc}$ should then be calculated from these strains as the mean stress via the room-pressure elastic tensor of quartz (e.g. Wang et al., 2015). This $P_{inc}$ can then be used in calculations based on the isotropic model for the evolution of host-inclusion systems (e.g. Angel et al., 2017) to calculate reliable $P_{trap}$ values. The intrinsic uncertainties and the correlation in the strains obtained in this way (e.g. Fig. 3) suggest that multiple measurements of a population of quartz inclusions trapped under the same conditions are required to obtain a statistically reliable estimate of $P_{trap}$ (as in Fig. 4).

**Acknowledgements:**

This project has received funding from the European Research Council (ERC) under the European Union's Horizon 2020 research and innovation programme (grant agreement No 714936) by M. Alvaro. MA has also been supported by the MIUR-SIR grant "MILE DEEp" (RBSI140351).

# REFERENCES


Alvaro, M., Luca, M.M., John, A.R., Mara, M., Nicola, C., Marco, S., Federica, M., Andrey, K., Marta, M., 2019. Quartz inclusions from eclogite xenoliths record past subduction. in prep.

Angel, R.J., Mazzucchelli, M.L., Alvaro, M., Nestola, F., 2017. EosFit-Pinc: A simple GUI for host-inclusion elastic thermobarometry. American Mineralogist 102, 1957-1960.

Angel, R.J., Mazzucchelli, M.L., Alvaro, M., Nimis, P., Nestola, F., 2014. Geobarometry from host-inclusion systems: The role of elastic relaxation. American Mineralogist 99, 2146-2149.

Angel, R.J., Murri, M., Mihailova, B., Alvaro, M., 2019. Stress, strain and Raman shifts. Zeitschrift fur kristallograhie - Crystalline Material 234, 11.

Angel, R.J., Nimis, P., Mazzucchelli, M.L., Alvaro, M., Nestola, F., 2015. How large are departures from lithostatic pressure? Constraints from host-inclusion elasticity. Journal of Metamorphic Geology 33, 801-813.

Ashley, K.T., Steele-MacInnis, M., Bodnar, R.J., Darling, R.S., 2016. Quartz-in-garnet inclusion barometry under fire: Reducing uncertainty from model estimates. Geology 44, 699-702.

Barron, T.H.K., Collins, J.F., Smith, T.W., White, G.K., 1982. Thermal expansion, Gruneisen functions and static lattice properties of quartz. Journal of Physics C: Solid State Physics 15, 4311-4326.

Barron, T.H.K., Collins, J.G., White, G.K., 1980. Thermal expansion of solids at low temperatures. Advances in Physics 29, 609-730.

Boyd, F.R., England, J.L., 1960. The quartz-coesite transition. Journal of Geophysical Research (1896-1977) 65, 749-756.

Campomenosi, N., Mazzucchelli, M.L., Mihailova, B.D., Scambelluri, M., Angel, R.J., Nestola, F., Reali, A., Alvaro, M., 2018. How geometry and anisotropy affect residual strain in host inclusion system: coupling experimental and numerical approaches. American Mineralogist 103, 2032-2035.

Cantrell, J.H., 1980. Generalized Grüuneisen tensor from solid nonlinearity parameters. Physical Review B 21, 4191-4195.

Enami, M., Nishiyama, T., Mouri, T., 2007. Laser Raman microspectrometry of metamorphic quartz: A simple method for comparison of metamorphic pressures. American Mineralogist 92, 1303-1315.

Grüneisen, E., 1926. Zustand des festen Körpers, in: Drucker, C., Grüneisen, E., Kohnstamm, P., Körber, F., Scheel, K., Schrödinger, E., Simon, F., van der Waals, J.D., Henning, F. (Eds.), Thermische Eigenschaften der Stoffe. Springer Berlin Heidelberg, Berlin, Heidelberg, pp. 1-59.

Holland, T., 1980. The reaction albite= jadeite+ quartz determined experimentally in the range 600–1200 C. American Mineralogist 65, 129-134.

Kitahara, S., Kennedy, G.C., 1964. The quartz-coesite transition. Journal of Geophysical Research (1896-1977) 69, 5395-5400.

Mazzucchelli, M.L., Burnley, P., Angel, R.J., Morganti, S., Domeneghetti, M.C., Nestola, F., Alvaro, M., 2018. Elastic geothermobarometry: Corrections for the geometry of the host-inclusion system. Geology 46, 231-234.

Mazzucchelli, M.L., Morganti, S., Reali, A., Chiara Domeneghetti, M., Angel, R.J., Alvaro, M., 2019. Elastic geobarometry: relaxation of elastically anisotropic inclusions.

Murri, M., Alvaro, M., Angel, R.J., Prencipe, M., Mihailova, B.D., 2019. The effects of non-hydrostatic stress on the structure and properties of alpha-quartz. Physics and Chemistry of Minerals.
Murri, M., Mazzucchelli, M.L., Campomenosi, N., Korsakov, A.V., Prencipe, M., Mihailova, B.D., Scambelluri, M., Angel, R.J., Alvaro, M., 2018. Raman elastic geobarometry for anisotropic mineral inclusions. American Mineralogist 103, 1869-1872.
Schmidt, C., Ziemann, M.A., 2000. In-situ Raman spectroscopy of quartz: A pressure sensor for hydrothermal diamond-anvil cell experiments at elevated temperatures. American Mineralogist 85, 1725-1734.
Spear, F.S., Thomas, J.B., Hallett, B.W., 2014. Overstepping the garnet isograd: a comparison of QuiG barometry and thermodynamic modeling. Contributions to Mineralogy and Petrology 168, 1059.
Thomas, J.B., Spear, F.S., 2018. Experimental study of quartz inclusions in garnet at pressures up to 3.0 GPa: evaluating validity of the quartz-in-garnet inclusion elastic thermobarometer. Contributions to Mineralogy and Petrology 173.
Trail, D., Bruce Watson, E., Tailby, N.D., 2012. Ce and Eu anomalies in zircon as proxies for the oxidation state of magmas. Geochimica et Cosmochimica Acta 97, 70-87.
Wang, J., Mao, Z., Jiang, F., Duffy, T.S., 2015. Elasticity of single-crystal quartz to 10 GPa. Physics and Chemistry of Minerals 42, 203-212.
Zhang, Y., 1998. Mechanical and phase equilibria in inclusion–host systems. Earth and Planetary Science Letters 157, 209-222.

## Figures

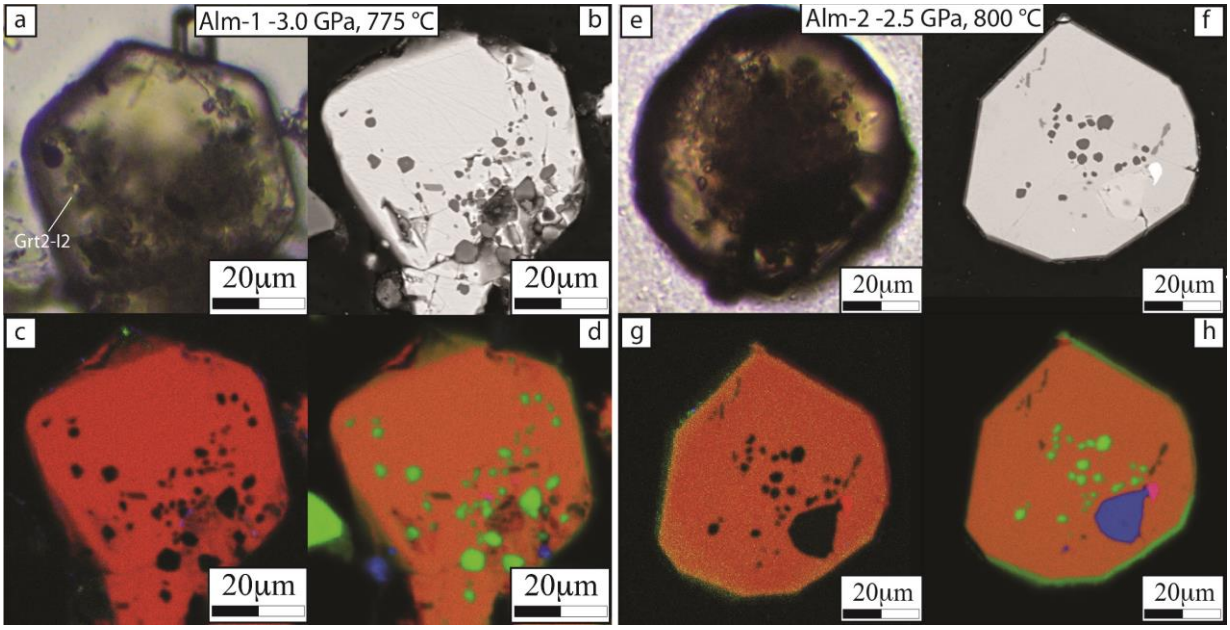


**Fig. 1**. Optical microphotographs and SEM-BSE image of the samples Alm-1 synthesized at 3.0GPa and 775°C and Alm-2 synthesized at 2.5GPa and 800°C.
(a,e) In optical microphotographs the garnets appear to be euhedral with several trapped inclusions. (b,f) Inclusions exposed on the surface are visible in the SEM-BSE images and therefore have not been used for further analyses. (c,g) The combined Fe-Mg-Ca chemical element maps in RGB show that almandine garnet is very homogeneous. (d,h) The combined Fe-Si-Ti chemical element maps in RGB show the different inclusion phases with quartz in green, rutile in blue and in pyroxene in pink.

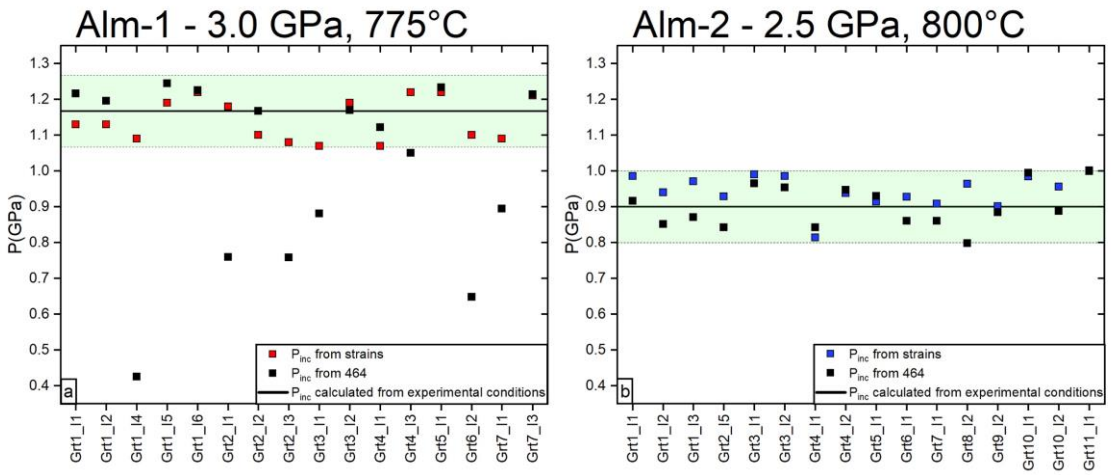


**Fig. 2.** Inclusion pressures calculated for the quartz inclusion in garnet from synthesis at 3.0 GPa (a, Alm-1) and 2.5GPa (b, Alm-2). The black line represents the inclusion pressure ($P_{inc}$) calculated from the synthesis conditions for quartz trapped in almandine garnet with the isotropic host-inclusion model, and the green shaded area represents the maximum allowed discrepancy following the uncertainties of the calculation. $P_{inc}$ calculated using the hydrostatic calibration ($P_{inc}^{464}, black\ squares$) from the shift of the 464 Raman band show a much larger discrepancy than those obtained from the strain components ($P_{inc}^{strains}, red\ squares$) for experiment at 3.0GPa (Alm-1). Much closer agreement between the two approaches has been obtained for the experiments at 2.5GPa (Alm-2, blue squares in part b).

328

329

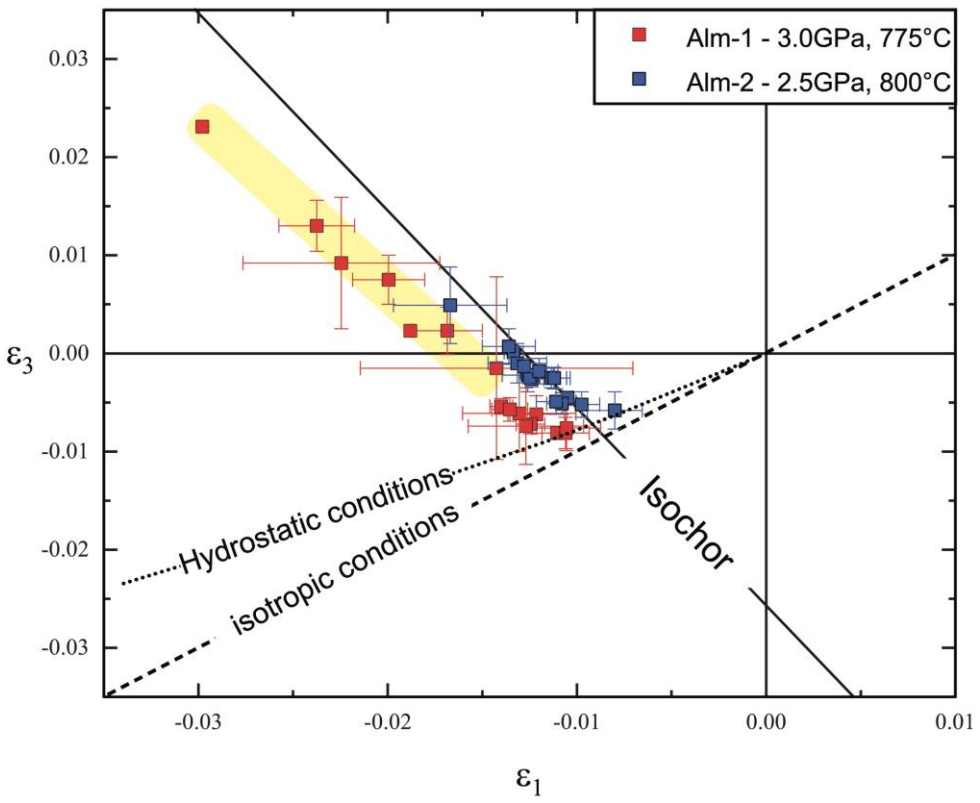


**Fig. 3.** Strain components determined at room temperature for quartz inclusions from experiments Alm-1 (red squares) and Alm-2 (blue squares). Lines for hydrostatic conditions (dotted), for isotropic conditions (dashed) and an isochor (filled) are also shown. The strains from both experiments lie almost parallel to the isochor and are clustered close to, but clearly above, the strains for hydrostatic conditions. The spread in values for the 2.5GPa experiment is much smaller than that for the inclusions synthesised at 3.0GPa. The yellow area indicates the inclusions in Alm-1 that have discrepancies in $P_{inc}^{464}$ larger than the experimental uncertainties (Fig. 2a).

330

331

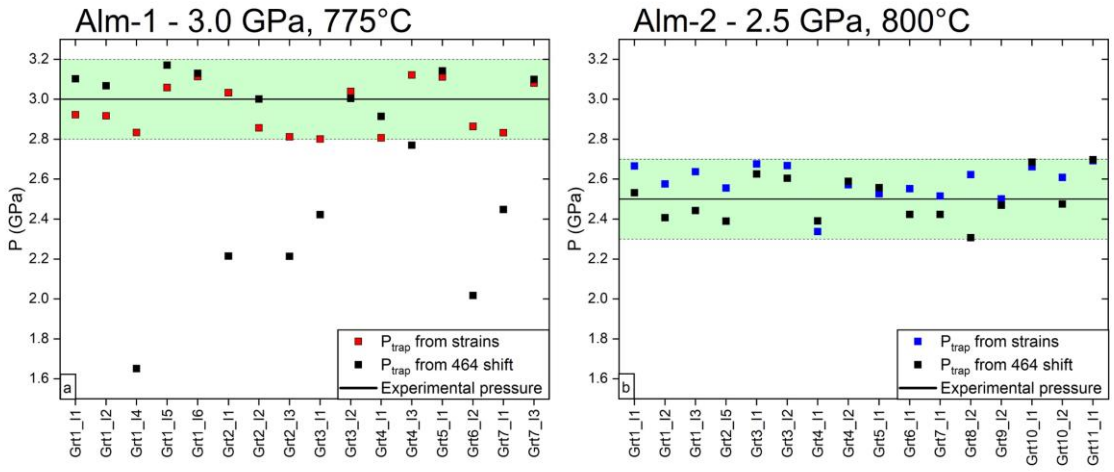


**Fig. 4.** Entrapment pressures calculated on the quartz inclusion in garnet synthesised at 3.0 GPa (a, Alm-1) and 2.5GPa (b, Alm-2). The black line represents the experimental pressure ($P_{trap}$) of the synthesis conditions for quartz trapped in almandine garnet and the green shaded area represents the maximum estimated uncertainty propagated through the calculation of $P_{trap}$. The uncertainty of the calibration of the piston cylinder is less than 0.02 GPa. $P_{trap}^{strains}$ obtained from $P_{trap}^{464}$ are represented by red squares and are in good agreement with experimental entrapment pressures for both experiments (Alm-1 and Alm-2). $P_{trap}^{464}$ ($black\ squares$) calculated from $P_{inc}^{464}$ showed a good agreement in the experiments at lower pressure and much larger spread in values in the experiment at higher pressure (Alm-1 3.0 GPa). The $P_{trap}^{464}$ values outside the uncertainty band are from the inclusions highlighted in yellow in Fig. 3.

## Tables

**Table 1a.** Raman peak positions and wavenumber shifts for quartz inclusions in garnet from experimental runs at 3.0 GPa and 775°C.

| | | | wave numbers ω(cm$^{-1}$) | | | | | | wave number shifts Δω (cm$^{-1}$) | | |
|---|---|---|---|---|---|---|---|---|---|---|---|
| **date** | **hosts** | **inclusions** | **128□(cm$^{-1}$)** | **e.s.d.** | **206 (cm$^{-1}$)** | **e.s.d.** | **464 (cm$^{-1}$)** | **e.s.d.** | **128 (cm$^{-1}$)** | **206 (cm$^{-1}$)** | **464 (cm$^{-1}$)** |
| **ideal inclusions** | | | | | | | | | | | |
| 05-12-18 | | I1 | 133.868 | 0.059 | 232.416 | 0.167 | 475.302 | 0.015 | 6.25 | 25.463 | 10.6 |
| 12-06-18 | | I2 | 132.878 | 0.266 | 231.051 | 0.36 | 474.503 | 0.041 | 5.643 | 25.089 | 10.432 |
| 12-06-18 | **Grt1** | I4 | 128.542 | 0.467 | 225.754 | 1.124 | 467.863 | 0.045 | 1.307 | 19.792 | 3.791 |
| 12-06-18 | | I5 | 133.722 | 0.171 | 232.654 | 0.296 | 474.918 | 0.034 | 6.487 | 26.692 | 10.846 |
| 12-06-18 | | I6 | 133.528 | 0.419 | 232.917 | 0.635 | 474.75 | 0.086 | 6.293 | 26.955 | 10.679 |
| 12-06-18 | | I1 | 131.968 | 0.306 | 229.953 | 0.861 | 470.771 | 0.058 | 4.733 | 23.992 | 6.699 |
| 05-12-18 | **Grt2** | I2 | 133.908 | 0.098 | 231.747 | 0.319 | 474.897 | 0.027 | 6.29 | 24.793 | 10.196 |
| 12-06-18 | | I3 | 131.177 | 0.619 | 227.919 | 1.181 | 470.769 | 0.07 | 3.942 | 21.957 | 6.697 |
| 05-12-18 | **Grt3** | I1 | 133.855 | 0.161 | 230.241 | 0.42 | 472.453 | 0.027 | 6.237 | 23.287 | 7.751 |
| 05-12-18 | | I2 | 134.292 | 0.056 | 233.304 | 0.163 | 474.911 | 0.073 | 6.674 | 26.35 | 10.209 |
| 12-06-18 | **Grt4** | I1 | 133.432 | 0.238 | 230.139 | 0.251 | 473.876 | 0.021 | 6.197 | 24.177 | 9.804 |
| 12-06-18 | | I3 | 132.264 | 0.289 | 231.796 | 0.461 | 473.271 | 0.073 | 5.029 | 25.834 | 9.199 |
| 05-12-18 | **Grt5** | I1 | 134.655 | 0.055 | 234.24 | 0.113 | 475.452 | 0.014 | 7.037 | 27.287 | 10.751 |
| 12-06-18 | **Grt6** | I2 | 130.461 | 0.324 | 227.636 | 0.954 | 469.815 | 0.043 | 3.226 | 21.674 | 5.743 |
| 27-11-18 | **Grt7** | I1 | 132.75 | 0.098 | 228.93 | 0.141 | 472.781 | 0.012 | 4.765 | 22.968 | 7.871 |
| 27-11-18 | | I3 | 134.328 | 0.09 | 232.656 | 0.295 | 475.499 | 0.032 | 6.343 | 26.694 | 10.589 |
| **not-ideal inclusions** | | | | | | | | | | | |
| 12-06-18 | **Grt1** | I2 | 131.534 | 0.376 | 223.81 | 0.691 | 471.938 | 0.039 | 4.299 | 17.848 | 7.867 |
| 12-06-18 | **Grt2** | I4 | 133.826 | 0.121 | 230.239 | 0.268 | 474.144 | 0.022 | 6.208 | 23.285 | 9.442 |
| 12-06-18 | | I2 | 131.239 | 0.879 | 233.673 | 0.682 | 473.886 | 0.133 | 4.004 | 27.711 | 9.815 |
| 12-06-18 | | I1 | 131.388 | 0.808 | 235.222 | 1.13 | 471.412 | 0.133 | 4.153 | 29.26 | 7.34 |
| 12-06-18 | **Grt6** | I3 | 132.091 | 0.161 | 225.545 | 0.934 | 472.481 | 0.041 | 4.856 | 19.583 | 8.409 |
| 12-06-18 | | I4 | 132.084 | 0.147 | 227.818 | 0.488 | 471.818 | 0.024 | 4.849 | 21.856 | 7.747 |
| 12-06-18 | **Grt7** | I2 | 134.341 | 0.101 | 234.468 | 0.225 | 475.36 | 0.029 | 6.356 | 28.506 | 10.451 |
| 12-06-18 | | I4 | 134.111 | 0.305 | 233.13 | 0.26 | 474.523 | 0.035 | 6.126 | 27.169 | 9.613 |

Note: Wavenumber shifts and their e.s.d.'s have been obtained as described in the text. Not-ideal inclusions cannot be used to calculate the entrapment pressure.

**Table 1b.** Raman peak positions and wavenumber shifts for quartz inclusions in garnet from experimental runs at 2.5 GPa and 800°C.

| | | | wave numbers ω(cm$^{-1}$) | | | | | | wave number shifts Δω (cm$^{-1}$) | | |
|---|---|---|---|---|---|---|---|---|---|---|---|
| **date** | **hosts** | **inclusions** | **128□(cm$^{-1}$)** | **e.s.d.** | **206 (cm$^{-1}$)** | **e.s.d.** | **464 (cm$^{-1}$)** | **e.s.d.** | **128 (cm$^{-1}$)** | **206 (cm$^{-1}$)** | **464 (cm$^{-1}$)** |
| **ideal inclusions** | | | | | | | | | | | |
| 07-12-18 | | I1 | 132.774 | 0.041 | 228.331 | 0.088 | 472.838 | 0.008 | 4.904 | 21.448 | 8.057 |
| 08-12-18 | **Grt1** | I2 | 131.907 | 0.042 | 226.990 | 0.080 | 472.279 | 0.006 | 4.037 | 20.107 | 7.498 |
| 09-12-18 | | I3 | 132.572 | 0.060 | 227.852 | 0.186 | 472.449 | 0.012 | 4.703 | 20.968 | 7.667 |
| 13-06-18 | **Grt2** | I5 | 131.705 | 0.102 | 227.078 | 0.224 | 472.206 | 0.017 | 3.737 | 19.767 | 7.416 |
| 05-12-18 | **Grt3** | I1 | 132.511 | 0.058 | 228.470 | 0.183 | 473.254 | 0.019 | 4.641 | 21.587 | 8.473 |
| 05-12-18 | | I2 | 132.481 | 0.059 | 228.348 | 0.214 | 473.160 | 0.017 | 4.611 | 21.464 | 8.379 |
| 07-12-18 | **Grt4** | I1 | 132.591 | 0.042 | 225.216 | 0.070 | 472.205 | 0.008 | 4.721 | 18.333 | 7.423 |
| 07-12-18 | | I2 | 132.723 | 0.032 | 227.654 | 0.117 | 473.099 | 0.008 | 4.853 | 20.770 | 8.318 |
| 07-12-18 | **Grt5** | I1 | 132.854 | 0.042 | 227.263 | 0.053 | 472.951 | 0.006 | 4.985 | 20.380 | 8.170 |
| 05-12-18 | **Grt6** | I1 | 132.413 | 0.047 | 227.041 | 0.234 | 472.357 | 0.015 | 4.543 | 20.158 | 7.576 |
| 07-12-18 | **Grt7** | I1 | 132.377 | 0.058 | 226.707 | 0.137 | 472.359 | 0.010 | 4.508 | 19.824 | 7.578 |
| 13-06-18 | **Grt8** | I2 | 130.914 | 0.209 | 227.137 | 1.184 | 471.827 | 0.046 | 2.946 | 19.826 | 7.037 |
| 22-11-18 | **Grt9** | I2 | 132.164 | 0.162 | 226.978 | 0.273 | 472.572 | 0.021 | 4.196 | 19.667 | 7.782 |
| 22-11-18 | **Grt10** | I1 | 133.222 | 0.067 | 229.171 | 0.283 | 473.518 | 0.024 | 5.254 | 21.860 | 8.728 |
| 22-11-18 | | I2 | 132.391 | 0.079 | 227.980 | 0.249 | 472.598 | 0.066 | 4.422 | 20.669 | 7.808 |
| 22-11-18 | **Grt11** | I1 | 133.301 | 0.043 | 229.476 | 0.156 | 473.573 | 0.017 | 5.332 | 22.164 | 8.783 |
| **not-ideal inclusions** | | | | | | | | | | | |
| 13-06-18 | **Grt2** | I4 | 131.462 | 0.165 | 226.831 | 0.278 | 472.199 | 0.019 | 3.493 | 19.520 | 7.409 |
| 13-06-18 | | I7 | 130.954 | 0.059 | 222.136 | 0.098 | 470.469 | 0.011 | 2.986 | 14.825 | 5.679 |
| 07-12-18 | **Grt4** | I2 | 133.604 | 0.063 | 230.322 | 0.152 | 473.950 | 0.017 | 5.734 | 23.438 | 9.169 |
| 07-12-18 | | I3 | 133.370 | 0.050 | 229.798 | 0.119 | 474.289 | 0.010 | 5.500 | 22.915 | 9.508 |
| 05-12-18 | **Grt6** | I2 | 133.223 | 0.050 | 229.927 | 0.150 | 473.721 | 0.014 | 5.353 | 23.044 | 8.940 |
| 22-11-18 | **Grt9** | I1 | 132.809 | 0.227 | 230.383 | 0.534 | 474.276 | 0.050 | 4.841 | 23.072 | 9.486 |
| 22-11-18 | | I3 | 133.353 | 0.115 | 230.690 | 0.355 | 473.992 | 0.033 | 5.384 | 23.379 | 9.202 |
| 22-11-18 | **Grt10** | I3 | 133.431 | 0.083 | 229.832 | 0.086 | 473.803 | 0.008 | 5.462 | 22.520 | 9.013 |
| 22-11-18 | **Grt11** | I2 | 132.998 | 0.047 | 229.855 | 0.158 | 473.749 | 0.013 | 5.029 | 22.544 | 8.959 |

**ALM2**

Note: Wavenumber shifts and their e.s.d.'s have been obtained as described in the text. Not-ideal inclusions cannot be used to calculate the entrapment pressure.

**Table 2a.** Calculated strains for quartz inclusions in garnet from experimental runs at 3.0 GPa and 775°C.

| | date | host | inclusion | $\varepsilon_1+\varepsilon_2$ | e.s.d. | $\varepsilon_3$ | e.s.d. | $\varepsilon_V$ | e.s.d. | Covariance (x$10^6$) | Correlation (%) | $\chi^2$ |
|---|---|---|---|---|---|---|---|---|---|---|---|---|
| | **ideal inclusions** | | | | | | | | | | | |
| **ALM1** | 05-12-18 | | I1 | -0.0221 | 0.0004 | -0.0081 | 0.0003 | -0.0302 | 0.0002 | -0.12 | -99 | 0.00 |
| | 12-06-18 | | I2 | -0.0243 | 0.0030 | -0.0062 | 0.0019 | -0.0305 | 0.0011 | -5.64 | -99 | 0.12 |
| | 12-06-18 | **Grt1** | I4 | -0.0596 | 0.0005 | 0.0231 | 0.0003 | -0.0365 | 0.0002 | -0.14 | -99 | 0.00 |
| | 12-06-18 | | I5 | -0.0249 | 0.0015 | -0.0072 | 0.0010 | -0.0322 | 0.0006 | -1.38 | -99 | 0.03 |
| | 12-06-18 | | I6 | -0.0280 | 0.0012 | -0.0054 | 0.0008 | -0.0333 | 0.0005 | -0.95 | -99 | 0.02 |
| | 12-06-18 | | I1 | -0.0449 | 0.0104 | 0.0092 | 0.0067 | -0.0358 | 0.0039 | -69.35 | -99 | 1.44 |
| | 05-12-18 | **Grt2** | I2 | -0.0212 | 0.0025 | -0.0081 | 0.0016 | -0.0293 | 0.0009 | -3.97 | -99 | 0.08 |
| | 12-06-18 | | I3 | -0.0399 | 0.0038 | 0.0075 | 0.0025 | -0.0324 | 0.0014 | -9.43 | -99 | 0.20 |
| | 05-12-18 | **Grt3** | I1 | -0.0285 | 0.0144 | -0.0015 | 0.0093 | -0.0300 | 0.0054 | - | -99 | 2.77 |
| | 05-12-18 | | I2 | -0.0261 | 0.0060 | -0.0061 | 0.0039 | -0.0322 | 0.0022 | -22.75 | -99 | 0.47 |
| | 12-06-18 | **Grt4** | I1 | -0.0211 | 0.0036 | -0.0076 | 0.0023 | -0.0287 | 0.0013 | -8.28 | -99 | 0.17 |
| | 12-06-18 | | I3 | -0.0376 | 0.0000 | 0.0023 | 0.0000 | -0.0353 | 0.0000 | 0.00 | -99 | 0.00 |
| | 05-12-18 | **Grt5** | I1 | -0.0254 | 0.0061 | -0.0074 | 0.0039 | -0.0328 | 0.0023 | -23.45 | -99 | 0.49 |
| | 12-06-18 | **Grt6** | I2 | -0.0475 | 0.0040 | 0.0130 | 0.0026 | -0.0345 | 0.0015 | -10.22 | -99 | 0.21 |
| | 27-11-18 | **Grt7** | I1 | -0.0337 | 0.0037 | 0.0023 | 0.0024 | -0.0314 | 0.0014 | -8.57 | -99 | 0.18 |
| | 27-11-18 | | I3 | -0.0271 | 0.0019 | -0.0057 | 0.0012 | -0.0328 | 0.0007 | -2.27 | -99 | 0.05 |
| | **not-ideal inclusions** | | | | | | | | | | | |
| | 12-06-18 | **Grt1** | I2 | -0.01341 | 0.00261 | -0.00712 | 0.00168 | -0.02053 | 0.00097 | -4.35 | -99 | 0.09 |
| | 12-06-18 | **Grt2** | I4 | -0.01916 | 0.00509 | -0.00807 | 0.00329 | -0.02723 | 0.00189 | -16.55 | -99 | 0.34 |
| | 12-06-18 | Grt4 | I2 | -0.04741 | 0.00908 | 0.00734 | 0.00586 | -0.04007 | 0.00338 | -52.71 | -99 | 1.1 |
| | 12-06-18 | | I1 | -0.06742 | 0.00627 | 0.01991 | 0.00405 | -0.04751 | 0.00233 | -25.13 | -99 | 0.52 |
| | 12-06-18 | **Grt6** | I3 | -0.01527 | 0.00072 | -0.00741 | 0.00046 | -0.02268 | 0.00027 | -0.33 | -99 | 0.01 |
| | 12-06-18 | | I4 | -0.02906 | 0.00421 | 0.0001 | 0.00272 | -0.02896 | 0.00157 | -11.36 | -99 | 0.24 |
| | 12-06-18 | **Grt7** | I2 | -0.0358 | 0.00384 | -0.00135 | 0.00248 | -0.03714 | 0.00143 | -9.41 | -99 | 0.2 |
| | 12-06-18 | | I4 | -0.03574 | 0.00599 | -0.00014 | 0.00387 | -0.03588 | 0.00223 | -22.98 | -99 | 0.48 |

Note: Values calculated using strainman software (Angel et al 2018) as described in the text. Not-ideal inclusions cannot be used to calculate the entrapment pressure.

**Table 2b.** Calculated strains for quartz inclusions in garnet from experimental runs at 2.5 GPa and 800°C. Values calculated using strainman software as described in the text.

ALM2

| date | host | inclusion | $\varepsilon_1+\varepsilon_2$ | e.s.d. | $\varepsilon_3$ | e.s.d. | $\varepsilon_V$ | e.s.d. | Covariance (x$10^6$) | Correlation (%) | $\chi^2$ |
|---|---|---|---|---|---|---|---|---|---|---|---|
| **ideal inclusions** | | | | | | | | | | | |
| 07-12-18 | | I1 | -0.0252 | 0.0027 | -0.0022 | 0.0017 | -0.0274 | 0.0010 | -4.52 | -99 | 0.09 |
| 08-12-18 | **Grt1** | I2 | -0.0267 | 0.0010 | 0.0001 | 0.0006 | -0.0267 | 0.0004 | -0.62 | -99 | 0.01 |
| 09-12-18 | | I3 | -0.0263 | 0.0031 | -0.0010 | 0.0020 | -0.0273 | 0.0012 | -6.19 | -99 | 0.13 |
| 13-06-18 | **Grt2** | I5 | -0.0272 | 0.0028 | 0.0007 | 0.0018 | -0.0265 | 0.0010 | -4.95 | -99 | 0.1 |
| 05-12-18 | **Grt3** | I1 | -0.0248 | 0.0013 | -0.0026 | 0.0008 | -0.0275 | 0.0005 | -1.05 | -99 | 0.02 |
| 05-12-18 | | I2 | -0.0250 | 0.0011 | -0.0024 | 0.0007 | -0.0274 | 0.0004 | -0.70 | -99 | 0.01 |
| 07-12-18 | **Grt4** | I1 | -0.0160 | 0.0029 | -0.0058 | 0.0019 | -0.0217 | 0.0011 | -5.51 | -99 | 0.11 |
| 07-12-18 | | I2 | -0.0210 | 0.0005 | -0.0045 | 0.0003 | -0.0255 | 0.0002 | -0.15 | -99 | 0 |
| 07-12-18 | **Grt5** | I1 | -0.0195 | 0.0019 | -0.0052 | 0.0013 | -0.0247 | 0.0007 | -2.39 | -99 | 0.05 |
| 05-12-18 | **Grt6** | I1 | -0.0240 | 0.0020 | -0.0018 | 0.0013 | -0.0259 | 0.0008 | -2.65 | -99 | 0.06 |
| 07-12-18 | **Grt7** | I1 | -0.0227 | 0.0016 | -0.0025 | 0.0010 | -0.0252 | 0.0006 | -1.59 | -99 | 0.03 |
| 13-06-18 | **Grt8** | I2 | -0.0334 | 0.0060 | 0.0049 | 0.0039 | -0.0285 | 0.0022 | -23.22 | -99 | 0.48 |
| 22-11-18 | **Grt9** | I2 | -0.0224 | 0.0017 | -0.0025 | 0.0011 | -0.0250 | 0.0006 | -1.91 | -99 | 0.04 |
| 22-11-18 | **Grt10** | I1 | -0.0216 | 0.0016 | -0.0051 | 0.0011 | -0.0267 | 0.0006 | -1.72 | -99 | 0.04 |
| 22-11-18 | | I2 | -0.0256 | 0.0003 | -0.0013 | 0.0002 | -0.0268 | 0.0001 | -0.05 | -99 | |
| 22-11-18 | **Grt11** | I1 | -0.0222 | 0.0021 | -0.0049 | 0.0013 | -0.0272 | 0.0008 | -2.70 | -99 | 0.06 |
| **not-ideal inclusions** | | | | | | | | | | | |
| 13-06-18 | **Grt2** | I4 | -0.0273 | 0.0045 | 0.0010 | 0.0029 | -0.0263 | 0.0017 | -13.17 | -99 | 0.27 |
| 13-06-18 | | I7 | -0.0188 | 0.0015 | -0.0006 | 0.0010 | -0.0194 | 0.0006 | -1.40 | -99 | 0.03 |
| 07-12-18 | **Grt4** | I2 | -0.0237 | 0.0035 | -0.0051 | 0.0022 | -0.0288 | 0.0013 | -7.67 | -99 | 0.16 |
| 07-12-18 | | I3 | -0.0206 | 0.0003 | -0.0068 | 0.0002 | -0.0274 | 0.0001 | -0.05 | -99 | 0 |
| 05-12-18 | **Grt6** | I2 | -0.0251 | 0.0019 | -0.0037 | 0.0012 | -0.0289 | 0.0007 | -2.28 | -99 | 0.05 |
| 22-11-18 | **Grt9** | I1 | -0.0247 | 0.0045 | -0.0041 | 0.0029 | -0.0288 | 0.0017 | -12.96 | -99 | 0.27 |
| 22-11-18 | | I3 | -0.0250 | 0.0009 | -0.0042 | 0.0006 | -0.0291 | 0.0003 | -0.50 | -99 | 0.01 |
| 22-11-18 | **Grt10** | I3 | -0.0219 | 0.0019 | -0.0055 | 0.0012 | -0.0274 | 0.0007 | -2.33 | -99 | 0.05 |
| 22-11-18 | **Grt11** | I2 | -0.0244 | 0.0007 | -0.0038 | 0.0005 | -0.0282 | 0.0003 | -0.32 | -99 | 0.01 |

Note: Values calculated using strainman software (Angel et al 2018) as described in the text. Not-ideal inclusions cannot be used to calculate the entrapment pressure.

**Table 3a.** Principal stress components ($\sigma_1=\sigma_2$ and $\sigma_3$), inclusion pressure (Pinc) and entrapment pressure (Ptrap) calculated for quartz inclusions in garnet from experimental runs at 3.0 GPa and 775°C.

**ALM1**

| | | | From 464 wavenumber shift | | From strain components | | | |
|---|---|---|---|---|---|---|---|---|
| **date** | **hosts** | **inclusions** | **Pinc (GPa)** | **Ptrap(GPa)** | **σ1=σ2 (GPa)** | **σ3 (GPa)** | **Pinc Δσ(GPa)** | **Ptrap(GPa)** |
| **ideal inclusions** | | | | | | | | |
| 05-12-18 | | I1 | 1.22 | 3.10 | -1.13 | -1.14 | 1.13 | 2.92 |
| 12-06-18 | | I2 | 1.20 | 3.07 | -1.21 | -0.96 | 1.13 | 2.92 |
| 12-06-18 | **Grt1** | I4 | 0.43 | 1.65 | -2.49 | 1.72 | 1.09 | 2.83 |
| 12-06-18 | | I5 | 1.24 | 3.17 | -1.25 | -1.08 | 1.19 | 3.06 |
| 12-06-18 | | I6 | 1.22 | 3.13 | -1.37 | -0.92 | 1.22 | 3.11 |
| 12-06-18 | | I1 | 0.76 | 2.22 | -1.98 | 0.42 | 1.18 | 3.03 |
| 05-12-18 | **Grt2** | I2 | 1.17 | 3.00 | -1.09 | -1.12 | 1.10 | 2.86 |
| 12-06-18 | | I3 | 0.76 | 2.21 | -1.77 | 0.30 | 1.08 | 2.81 |
| 05-12-18 | **Grt3** | I1 | 0.88 | 2.42 | -1.35 | -0.51 | 1.07 | 2.80 |
| 05-12-18 | | I2 | 1.17 | 3.00 | -1.29 | -0.97 | 1.19 | 3.04 |
| 12-06-18 | **Grt4** | I1 | 1.12 | 2.91 | -1.08 | -1.07 | 1.07 | 2.81 |
| 12-06-18 | | I3 | 1.05 | 2.77 | -1.72 | -0.22 | 1.22 | 3.12 |
| 05-12-18 | **Grt5** | I1 | 1.23 | 3.14 | -1.28 | -1.10 | 1.22 | 3.11 |
| 12-06-18 | **Grt6** | i2 | 0.65 | 2.018 | -2.05 | 0.80 | 1.10 | 2.86 |
| 27-11-18 | **Grt7** | I1 | 0.89 | 2.448 | -1.54 | -0.18 | 1.09 | 2.83 |
| 27-11-18 | | I3 | 1.21 | 3.1 | -1.34 | -0.95 | 1.21 | 3.08 |
| **not-ideal inclusions** | | | | | | | | |
| 12-06-18 | **Grt1** | I2 | 0.89 | 2.466 | -0.71 | -0.92 | 0.78 | 2.24 |
| 12-06-18 | **Grt2** | I4 | 1.08 | 2.815 | -0.99 | -1.10 | 1.03 | 2.71 |
| 12-06-18 | **Grt4** | I2 | 1.12 | 2.917 | -2.12 | 0.19 | 1.35 | 3.40 |
| 12-06-18 | | I1 | 0.83 | 2.352 | -2.90 | 1.28 | 1.51 | 3.76 |
| 12-06-18 | **Grt6** | I3 | 0.96 | 2.588 | -0.80 | -0.98 | 0.86 | 2.39 |
| 12-06-18 | | I4 | 0.88 | 2.44 | -1.35 | -0.35 | 1.02 | 2.69 |
| 12-06-18 | **Grt7** | I2 | 1.20 | 3.066 | -1.69 | -0.59 | 1.32 | 3.34 |
| 12-06-18 | | I4 | 1.10 | 2.856 | -1.67 | -0.46 | 1.27 | 3.21 |

Note: Principal stress components have been calculated using the full elastic tensor by Wang et al. (2015)) as described in the text. Values of Pinc have been calculated from the stress components as described in the text. Ptrap values have been calculated using EosFit-Pinc ((Angel et al., 2017)). Not ideal inclusions show the wrong pressure, the problems can be a lot , for example they are partially exposed or to be close the host boundary or to be close fracture.

**Table 3b** Principal stress components ($\sigma_1=\sigma_2$ and $\sigma_3$), inclusion pressure (Pinc) and entrapment pressure (Ptrap) calculated for quartz inclusions in garnet from experimental runs at 2.5 GPa and 800°C.

ALM2

| | | | From 464 wavenumber shift | | From strain components | | | |
|---|---|---|---|---|---|---|---|---|
| **date** | **hosts** | **inclusions** | **Pinc (GPa)** | **Ptrap(GPa)** | **σ1=σ2 (GPa)** | **σ3 (GPa)** | **Pinc Δσ(GPa)** | **Ptrap(GPa)** |
| **ideal inclusions** | | | | | | | | |
| 07-12-18 | | I1 | 0.92 | 2.532 | -1.20 | -0.54 | 0.98 | 2.67 |
| 08-12-18 | **Grt1** | I2 | 0.85 | 2.407 | -1.25 | -0.33 | 0.94 | 2.58 |
| 09-12-18 | | I3 | 0.87 | 2.443 | -1.24 | -0.43 | 0.97 | 2.64 |
| 13-06-18 | **Grt2** | I5 | 0.84 | 2.39 | -1.26 | -0.27 | 0.93 | 2.56 |
| 05-12-18 | **Grt3** | I1 | 0.97 | 2.626 | -1.19 | -0.59 | 0.99 | 2.68 |
| 05-12-18 | | I2 | 0.95 | 2.605 | -1.19 | -0.57 | 0.99 | 2.67 |
| 07-12-18 | **Grt4** | I1 | 0.84 | 2.391 | -0.82 | -0.81 | 0.81 | 2.34 |
| 07-12-18 | | I2 | 0.95 | 2.589 | -1.04 | -0.74 | 0.94 | 2.57 |
| 07-12-18 | **Grt5** | I1 | 0.93 | 2.557 | -0.97 | -0.79 | 0.91 | 2.53 |
| 05-12-18 | **Grt6** | I1 | 0.86 | 2.424 | -1.14 | -0.49 | 0.93 | 2.55 |
| 07-12-18 | **Grt7** | I1 | 0.86 | 2.424 | -1.09 | -0.54 | 0.91 | 2.52 |
| 13-06-18 | **Grt8** | I2 | 0.80 | 2.307 | -1.50 | 0.11 | 0.96 | 2.62 |
| 22-11-18 | **Grt9** | I2 | 0.88 | 2.47 | -1.08 | -0.55 | 0.90 | 2.50 |
| 22-11-18 | **Grt10** | I1 | 1.00 | 2.685 | -1.07 | -0.81 | 0.98 | 2.66 |
| 22-11-18 | | I2 | 0.89 | 2.476 | -1.21 | -0.45 | 0.96 | 2.61 |
| 22-11-18 | **Grt11** | I1 | 1.00 | 2.698 | -1.10 | -0.80 | 1.00 | 2.69 |
| **not-ideal inclusions** | | | | | | | | |
| 13-06-18 | **Grt2** | I4 | 0.84 | 2.388 | -1.29 | -0.44 | 1.01 | 2.71 |
| 13-06-18 | | I7 | 0.64 | 2.03 | -0.89 | -0.30 | 0.69 | 2.11 |
| 07-12-18 | **Grt4** | I2 | 1.05 | 2.789 | -1.17 | -0.83 | 1.06 | 2.81 |
| 07-12-18 | | I3 | 1.09 | 2.87 | -1.05 | -0.97 | 1.02 | 2.74 |
| 05-12-18 | **Grt6** | I2 | 1.02 | 2.734 | -1.22 | -0.71 | 1.05 | 2.79 |
| 22-11-18 | **Grt9** | I1 | 1.08 | 2.865 | -1.20 | -0.74 | 1.05 | 2.80 |
| 22-11-18 | | I3 | 1.05 | 2.797 | -1.22 | -0.75 | 1.06 | 2.82 |
| 22-11-18 | **Grt10** | I3 | 1.03 | 2.753 | -1.09 | -0.86 | 1.01 | 2.72 |
| 22-11-18 | **Grt11** | I2 | 1.02 | 2.738 | -1.19 | -0.71 | 1.03 | 2.75 |

Note: Principal stress components have been calculated using the full elastic tensor by Wang et al. (2015)) as described in the text. Values of Pinc have been calculated from the stress components as described in the text. Ptrap values have been calculated using EosFit-Pinc ((Angel et al., 2017)). Not ideal inclusions show the wrong pressure, the problems can be a lot , for example they are partially exposed or to be close the host boundary or to be close fracture.

S1 composition of oxides mixture used to synthesise garnet with quartz inclusions

**starting material (QuiG 13-02-16)**

| oxide | wt% |
|---|---|
| SiO2 | 59,23 |
| Al2O3 | 15,39 |
| FeO | 10,1 |
| Fe2O3 | 8,13 |
| TiO2 | 7,16 |

composition of buffer used to control oxygen fugacity of experiments

**FMQ**

| oxide | wt% |
|---|---|
| SiO2 | 23,43 |
| FeO | 38,59 |
| Fe3O4 | 37,98 |

1

S2 Quartz reference

| | DATE | STANDARD | SAMPLE | location | 128 ($cm^{-1}$) | e.s.d. | 206 ($cm^{-1}$) | e.s.d. | 464 ($cm^{-1}$) | e.s.d. |
|---|---|---|---|---|---|---|---|---|---|---|
| ALM1 | 12-06-18 | quartz thin section | THIN SECTION | eclogitic_ Fjordorf | 127.235 | 0.038 | 205.962 | 0.046 | 464.072 | 0.016 |
| | 27-11-18 | quartz thin section | THIN SECTION | granite_Ivrea Verbano Zone | 127.985 | 0.021 | 207.236 | 0.064 | 464.910 | 0.006 |
| | 05-12-18 | quaryz free crystal | FREE CRYSTAL | unknow | 127.617 | 0.026 | 206.954 | 0.066 | 464.702 | 0.006 |
| ALM2 | 13-06-18 | quartz thin section | THIN SECTION | Eclogitic_ Fjordorf | 126.648 | 0.023 | 205.319 | 0.036 | 463.480 | 0.009 |
| | 22-11-18 | quartz thin section | THIN SECTION | granite- Ivrea Verbano Zone | 127.969 | 0.019 | 207.311 | 0.059 | 464.790 | 0.010 |
| | 05-12-18 | quaryz free crystal | FREE CRYSTAL | unknow | 127.870 | 0.023 | 206.883 | 0.055 | 464.781 | 0.006 |

2

3

4

5
6